Title
Depth determination of chromophores in human skin by pulsed photothermal radiometry.

Journal
Applied Optics, 35(19)

ISSN
0003-6935

Authors
Milner, Thomas E
Smithies, Derek J
Goodman, Dennis M
et al.

Publication Date
1996-07-01

DOI
10.1364/ao.35.003379

Depth determination of chromophores in human skin by pulsed photothermal radiometry

Thomas E. Milner, Derek J. Smithies, Dennis M. Goodman, Alice Lau, and J. Stuart Nelson

We report on the application of pulsed photothermal radiometry (PPTR) to determine the depth of *in-vitro* and *in-vivo* subsurface chromophores in biological materials. Measurements provided by PPTR in combination with a nonnegative constrained conjugate-gradient algorithm are used to determine the initial temperature distribution in a biological material immediately following pulsed laser irradiation. Within the experimental error, chromophore depths (50–450 μm) in 55 *in-vitro* collagen phantoms determined by PPTR and optical low-coherence reflectometry are equivalent. The depths of port-wine-stain blood vessels determined by PPTR correlate very well with their locations found by computer-assisted microscopic observation of histologic sections. The mean blood-vessel depth deduced from PPTR and histologic observation is statistically indistinguishable ($p > 0.94$).

1. Introduction

In recent years, a number of investigators have studied various techniques to image the internal structure of human skin.[1–3] Many of these studies have been motivated by efforts to improve diagnosis and treatment of various skin pathologies. The increased use of lasers for medical treatments that rely on a photothermal-damage mechanism has heightened interest in infrared diagnostic methods. In many cases, information deduced from an infrared diagnostic measurement can be applied directly for improved therapeutic results.

Pulsed photothermal radiometry (PPTR) is a noncontact technique that utilizes an infrared detector to measure temperature changes induced in a test material exposed to pulsed radiation. Heat generated as a result of light absorption by subsurface chromophores in the test material diffuses to the surface and results in increased infrared emission levels. By the collection and concentration of the emitted radiation onto an infrared detector, a PPTR signal is obtained that represents the time evolution of temperature near the test-material surface. Useful information regarding the test material may be deduced from analysis of the PPTR signal; reported applications include (1) evaluation of surface-coating thickness in industrial components,[4] (2) identification of subsurface microcracks in aircraft structures,[5] (3) determination of the optical absorption coefficients in human artery[6] and biliary calculi,[7] and (4) characterization of vascular lesions in human skin, such as port-wine stain (PWS) birthmarks.[8]

Various investigators have reported mathematical and physical methods to deduce the optical and thermal properties of a laser-irradiated test material from a PPTR measurement. By using tissue phantoms that permit the independent variation of the optical absorption μ_a and scattering μ_s coefficients, Anderson *et al.*[9] found that heating of superficial layers increases when μ_s is greater. Prahl *et al.*[10] derived an analytic expression for the PPTR signal amplitude in terms of the optical and thermal properties of the irradiated test material and obtained estimates of μ_a and μ_s. Vitkin *et al.*[11] extended the analysis of Prahl *et al.*[10] to a generalized two-layer model and applied their results to PWS diagnostics. Milner *et al.*[12] used a numerical-

T. E. Milner, D. J. Smithies, and J. S. Nelson are with the Beckman Laser Institute and Medical Clinic, and J. S. Nelson is also with the Departments of Dermatology and Surgery, University of California, Irvine, Irvine, California 92715. D. M. Goodman is with the Lawrence Livermore National Laboratory, Livermore, California 94550; and A. Lau is with the Finch University of Health Sciences/The Chicago Medical School, North Chicago, Illinois 60637. T. E. Milner is also with the Department of Physics, Harvey Mudd College, Claremont, California 91711.

Received 13 November 1995.
0003-6935/96/193379-07$10.00/0

inversion algorithm to compute the initial temperature distribution in a test material from a PPTR signal recorded immediately following pulsed laser irradiation.

In this paper we report the results of an experimental investigation to determine the depth of *in-vitro* and *in-vivo* subsurface chromophores in biological materials from measurements provided by PPTR. An *in-vitro* phantom that makes use of thin, type I collagen films is used to simulate a subsurface chromophore positioned at various depths in human skin. The recorded PPTR signal amplitude in combination with a nonnegative constrained conjugate-gradient inversion algorithm is used to deduce the chromphore depth in the phantom and is compared with locations measured by the use of optical low-coherence reflectometry (OLCR).

In human skin, heat generated from the absorption of laser radiation by melanin and hemoglobin diffuses to the surface and results in increased infrared emission levels. In experiments similar to those using collagen phantoms, the recorded PPTR signal amplitude in combination with the nonnegative constrained conjugate-gradient inversion algorithm is used to deduce the depth of dermal PWS blood vessels and is compared with values deduced from a computer-assisted microscopic examination of histologic sections.

2. Theory

When the diameter of the laser-irradiation spot is much larger than the thermal-diffusion length, heat transport in the test material along the z axis is well approximated by a one-dimensional model (Fig. 1). In this case, the measured PPTR signal amplitude $\Delta S(t)$ is related to the initial temperature distribution $\Delta T(z, t = 0)$ in the test material immediately following pulsed laser irradiation by a Fredholm integral equation of the first kind, Eqs. (1)[12]:

$$\Delta S(t) = \int_z \Delta T(z, t = 0) K(z, t) \mathrm{d}z + n(t),$$

$$K(z, t) = \frac{\mu_{ir}}{2} \exp(-z^2/4Dt) \times \left\{ \mathrm{erfcx}(u_+) + \mathrm{erfcx}(u_-) - \frac{2h/\kappa}{h/\kappa - \mu_{ir}} \times [\mathrm{erfcx}(u_+) - \mathrm{erfcx}(u_1)] \right\}. \quad (1)$$

Here, $\mathrm{erfcx}(u) = [\exp(u^2)][\mathrm{erfc}(u)]$ is the exponential complementary error function; high-accuracy (18 digits) computation of $\mathrm{erfcx}(u)$ is possible by the use of a Chebyshev approximation.[13] Both $\Delta S(t)$ (in degrees Celsius) and $\Delta T(z, t = 0)$ (also in degrees Celsius) represent temperature increases relative to their respective background levels just before laser irradiation, i.e., $\Delta S(t) = S(t) - S(t = 0^-)$ and $\Delta T(z, t = 0) = T(z, t = 0) - T(z, t = 0^-)$, where $t = 0^-$ is the time just before laser irradiation. $K(z, t)$ is the kernel of the integral equation, $n(t)$ represents system noise, and $u_\pm$ and u_1 are defined as

$$u_\pm = \mu_{ir}\sqrt{Dt} \pm z/2\sqrt{Dt}, \quad u_1 = \frac{h}{\kappa}\sqrt{Dt} + z/\sqrt{Dt}, \quad (2)$$

respectively, where D (mm^2/s) is the thermal diffusivity of the irradiated test material, μ_{ir} (mm^{-1}) is the infrared absorption coefficient, κ ($\mathrm{W/mm^2\ K}$) is the thermal conductivity, and h [in watts per (millimeters squared times degrees kelvin)] is the heat-loss coefficient at the air–material boundary.

Given a measured PPTR signal $\Delta S(t)$, a unique solution for $\Delta T(z, t = 0)$ does not exist because the Fredholm integral equation is severely ill posed.[14] Equivalently, the kernel $K(z, t)$ strongly blurs the initial temperature distribution, so that accurate reconstruction of $\Delta T(z, t = 0)$ from the measured PPTR signal amplitude $\Delta S(t)$ requires an unrealistically-large signal-to-noise ratio. Inasmuch as a temperature change in response to light absorption is always positive, improved solution estimates are obtained by the imposition of a nonnegativity constraint [i.e., $\Delta T(z, t = 0) \geq 0$].

When finding a solution estimate for the initial temperature distribution $\Delta T(z, t = 0)$, the Fredholm integral equation [Eqs. (1)] is linearized, and one seeks to minimize a regularized norm:

$$f(\Delta \mathbf{T}, \Lambda) = \min[\|\mathbf{K}\Delta\mathbf{T} - \Delta\mathbf{S}\|^2 + \Lambda\|\Delta\mathbf{T}\|^2]. \quad (3)$$

Here $\Delta\mathbf{S}$ and $\Delta\mathbf{T}$ are linearized vector quantities representing the PPTR signal amplitude $\Delta S(t)$ and the initial temperature distribution $\Delta T(z, t = 0)$, respectively. The linearized kernel of the integral equation is represented by the matrix $\mathbf{K}$. A regular-

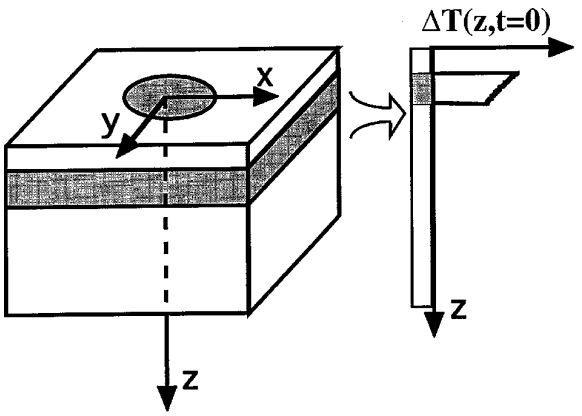

Fig. 1. Three-dimensional phantom geometry approximated as a one-dimensional model with the initial temperature distribution $\Delta T(z, t = 0)$. The oval shaded region represents the laser-irradiation spot.

ization term,[14] $\Lambda\|\Delta\mathbf{T}\|^2$, is added to the squared norm of the residual $\|\mathbf{K}\Delta\mathbf{T} - \Delta\mathbf{S}\|^2$ to penalize large solution estimates. We apply a nonnegative constrained conjugate-gradient algorithm to the unaugmented problem ($\Lambda = 0$) of Eq. (3), starting with $\Delta\mathbf{T} = 0$, and then regularize by early termination.[12,15] In the chemometrics literature this method is called the partial least-squares technique and has been given a sound theoretical basis.[16,17] Although the best iterate can be selected by the use of ordinary or generalized cross validation,[18] in our analysis both the discrepancy-principle[14] and the *L*-curve methods[19] are used to determine the best iterate.

3. Methods and Materials

We have developed an *in-vitro* model using thin, type I collagen films consisting of variable amounts of organic absorbing dye to simulate multilayered composite PWS skin (Fig. 1). The collagen films were prepared to different thicknesses and optical absorptions to simulate a PWS. We constructed each phantom by staining a single collagen film with triphenylmethane dye (Brilliant Blue, Aldrich Chemical Company) which absorbs optimally at a wavelength of 585 nm. We prepared each phantom by first placing a stained film on a 10-mm-thick collagen substrate to simulate the optical and thermal properties of the dermis and second by positioning a variable number (1–4) of unstained films over the stained layer to simulate a PWS with blood vessels at various depths (50–450 μm).

Before and after each PPTR measurement, the depth of the stained collagen film was determined by means of OLCR. The physical principles underlying OLCR have been described previously by many investigators[20–22] and are not given here. Briefly, OLCR utilizes a low-coherence Michelson interferometer to measure the backscattered-light amplitude at discrete user-specified depths within a turbid material. Each OLCR scan of the collagen phantom measured the amplitude of the backscattered light at increasing depths. Because of a discontinuity in the refractive index, the boundaries between adjacent collagen films were detected in the OLCR scan as peaks in the backscattered-light amplitude. Knowledge of the group refractive index of collagen and the position of the backscattering peaks permitted accurate depth determinations of the stained collagen film.

In experiments involving phantoms, light emitted by a flash-lamp-pumped, pulsed dye laser (0.45 ms, $E_p = 0.5$ J, $\lambda = 585$ nm) was imaged from a 1-mm core-diameter multimode optical fiber onto the collagen surface at 30° from the sample normal to form a 25-mm^2 elliptically-shaped irradiation spot. A 25-mm-diameter $f/1$ germanium lens stopped down to 5 mm was positioned 50 mm in front of the detector to provide the unit magnification (Fig. 2). Infrared radiation emitted from the phantom was amplitude modulated (3.9 kHz) by a mechanical chopper positioned at the 5-mm-diameter aperture and imaged onto a 1-mm^2 liquid-nitrogen-cooled HgCdTe detector optically filtered at the cold stop for sensitivity in the 10–14-μm spectral range. The detected signal was demodulated by a lock-in amplifier (Model SR850, Stanford Research Systems), recorded by a digital oscilloscope (Model DSA 601, Tektronix), and transferred to a magneto-optic storage disk.

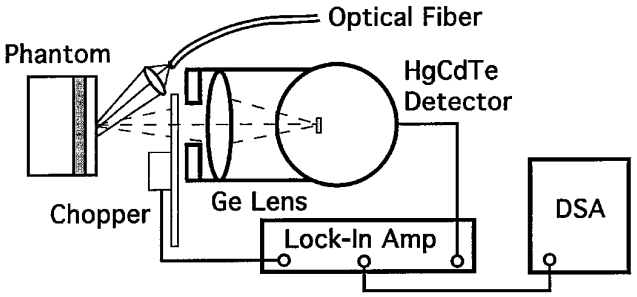

Fig. 2. Schematic of the apparatus used to record PPTR signals in experiments involving phantoms.

Following University of California internal review board approval, informed consent to participate in the study was given by three PWS patients undergoing laser therapy at the Beckman Laser Institute and Medical Clinic. In experiments involving PWS's, light emitted by a flash-lamp-pumped, pulsed dye laser (0.45 ms, $E_p = 1.5$ J, $\lambda = 585$ nm) was imaged from a 1-mm core-diameter multimode optical fiber at 30° from the normal to form a 25-mm^2 elliptically shaped irradiation spot on the skin surface. Infrared emission from the PWS was imaged onto a liquid-nitrogen-cooled 128 × 128 InSb infrared focal-plane array (IR-FPA) camera (Model AE 4128, Amber Engineering). The camera optics consisted of an $f/3$ multi-element infrared lens and filter positioned at the cold stop to limit the sensitivity to the 3–5-μm spectral range. The PWS was held stationary against the insulated back surface of a 20-mm-diameter iris diaphragm positioned 190 mm from the lens objective to yield an image-to-object linear magnification of 0.4. PWS sites ranging in appearance from light red or pink to purple were selected for laser irradiation; an adjacent normally pigmented skin site was also irradiated and served as the control. Immediately following the pulsed laser irradiation, 140 infrared emission images were recorded (217 frames/s) and transferred to a magneto-optic storage disk. From the more than 50 recorded PPTR signals of PWS's, patient consent permitted the biopsy of seven skin sites.

Immediately after surgical removal from the skin, tissue samples were fixed for 24 h in a phosphate buffer (pH 7.4), 10% formalin solution. Each tissue sample was sequentially dehydrated in 10 solutions of increasing ethanol:water concentrations, cleared (Histoclear, National Diagnostics), and then infiltrated with paraffin in an automated processor (Model 166 MP, Fisher Scientific). After the tissue samples were embedded in 1-cm^3 paraffin blocks, 6-μm-thick

serial sections were cut and placed on a clean glass slide. Sections were cleared of paraffin, stained with hematoxylin and eosin, and protected with a coverglass.

4. Results and Discussion

The nonnegative constrained conjugate-gradient inversion algorithm was used to analyze PPTR signals recorded from collagen phantoms and PWSs; the value of thermal diffusivity for each inversion was 0.11 mm^2/s.[23] When working with collagen phantoms, we took the magnitude of the infrared absorption coefficient (100 mm^{-1}) from the values for water[24,25] and collagen,[26] averaged over the spectral response of the HgCdTe detector (i.e., 10–14 μm). Air currents generated by the mechanical chopper required the use of a nonzero heat-loss coefficient. A value of h [23 $W/(m^2\ K)$] as determined by the computation of a least-squares fit to the tail of the recorded PPTR signals was consistent with values for forced-air convective cooling.[27] After a number of computer experiments with the simulated data, a criterion was derived [see Eq. (4)] to locate the position z_c of the upper surface of the stained collagen film from $\Delta T(z, t = 0)$:

$$z_c = \min\{z : \Delta T(z, t = 0) = 0.85\Delta T_{\max}\}, \qquad (4)$$

where $\Delta T_{\max}$ is the maximum temperature of $\Delta T(z, t = 0)$. For each collagen phantom, the PPTR signal amplitude [Fig. 3(a)] was used to compute z_c by the application of the nonnegative constrained conjugate-gradient inversion algorithm [Fig. 3(b), $\Delta T(z, t = 0)$] and the criterion in Eq. (4). With the group refractive index of collagen ($n_g = 1.43$),[28] z_c was determined from OLCR measurements. Of the 55 collagen phantoms tested, the standard deviation of the difference between values of z_c deduced by the use of the two methods was 2 μm (Fig. 4).

PPTR signals representing the thermal response of normal and PWS skin were derived from recorded infrared emission images by the computation of the average temperature within a 3-mm-diameter circular area centered in the elliptical-shaped irradiation spot. For inversions involving human skin, the infrared absorption coefficient (35 mm^{-1}) was deduced from the values for water[24,25] and collagen[26] averaged over the spectral response (i.e., 3–5 μm) of the IR-FPA camera. Because PPTR measurements of PWS's with the IR-FPA did not require a mechanical chopper, heat loss at the skin surface was dominated by unforced air convection [$h = 1\ W/(m^2\ K)$].[27] Tested skin sites were categorized according to appearance into one of three types: I, a deep red or purple PWS; II, a light red PWS; and III, natural or normal pigmentation.

Recorded PPTR signals representative of each skin type [Fig. 5(a)] indicate differences in the thermal response following pulsed laser irradiation. As noted previously,[8] the initial thermal response of skin immediately following pulsed laser irradiation

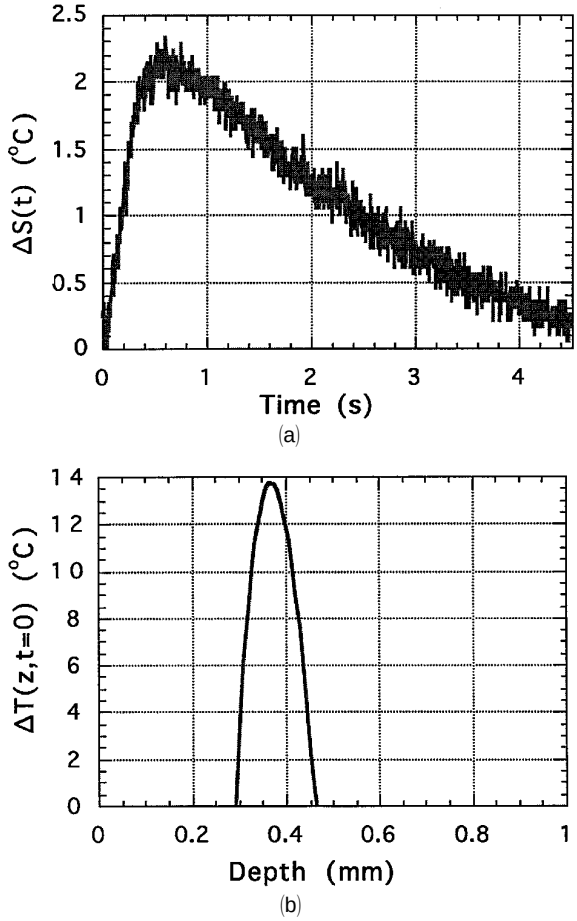

Fig. 3. Representative signals from an *in-vitro* collagen phantom: (a) PPTR signal amplitude $\Delta S(t)$, and (b) computed initial temperature distribution $\Delta T(z, t = 0)$, with $z_c = 0.33$ mm.

is dominated by epidermal melanin heating. A delayed thermal wave caused by heat deposited in deeper chromophores diffuses to the skin surface and produces increased temperatures. We expect, and our measurements confirm, that heat deposited

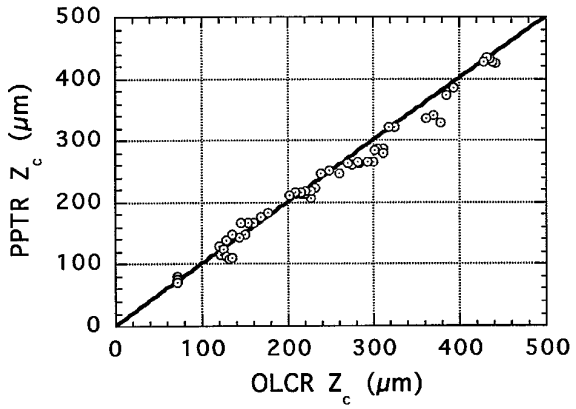

Fig. 4. Depth of the upper surface (z_c) of a stained collagen film deduced from the inversion of the PPTR signal and the OLCR measurement: The solid line represents the case of PPTRz_c = OLCRz_c; the center-dot circles represent individual data points.

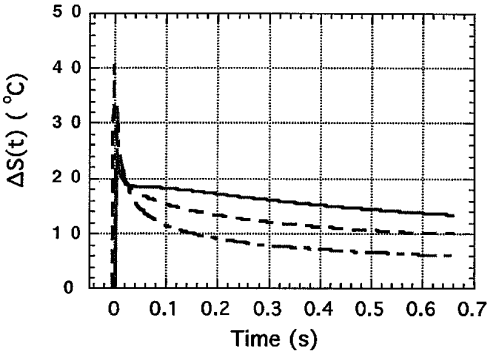

(a)

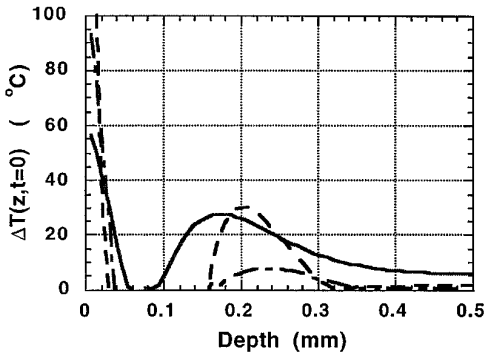

(b)

Fig. 5. Representative signals from three skin types exposed to equivalent laser irradiance: solid curves, type I skin; dashed curves, type II skin; short-dash–long-dash curves, type III skin. The plots show the (a) PPTR signal amplitude $\Delta S(t)$, and (b) computed initial temperature distribution $\Delta T(z, t = 0)$.

in dermal PWS blood vessels results in an increased PPTR signal amplitude at later times (~0.7 s). At these times, the recorded amplitude from type I sites is greatest; in contrast, the amplitude of type III sites decays more rapidly and attains the smallest relative magnitude at later times.

The initial temperature distribution $\Delta T(z, t = 0)$ corresponding to each laser-irradiated and biopsied skin site was computed by the application of the nonnegative constrained conjugate-gradient inversion algorithm. Distinct regions of increased temperature in the epidermis and dermis are evident and indicate light absorption by melanin and hemoglobin, respectively, contained within the PWS blood vessels. The computation of $\Delta T(z, t = 0)$ for the three representative PPTR signals illustrated in Fig. 5(a) indicates that heat generated in dermal PWS blood vessels is greatest in type I sites and decreases monotonically for skin types II and III [Fig. 5(b)]. Over the seven biopsied skin sites, the mean peak temperature increases of the subsurface blood vessels for skin types I, II, and III are 34, 27, and 8 °C, respectively.

Microscopic observation of the histologic sections permitted the comparison of PWS blood-vessel locations with their corresponding initial temperature distributions, $\Delta T(z, t = 0)$. An electronic camera (Model 2250, Cidtec) in combination with a low-power (10×) microscope (Model BH-2, Olympus) were used to record digital images (512 × 512 pixels) of 20 equal-spaced tissue sections taken from each skin biopsy. With a computer-assisted analysis of the recorded histologic images, the (x, z) coordinates representing the periphery of each PWS blood vessel were identified by a manual trace of a closed geometric curve coincident with the venule boundary. The depth of each PWS blood vessel was taken to be the distance along a line segment connecting the center position (x_c, z_c) to the nearest point on the skin surface, as given by

$$x_c = \frac{x_{\min} + x_{\max}}{2}, \qquad z_c = \frac{z_{\min} + z_{\max}}{2}. \tag{5}$$

For each biopsied skin site a histogram representing the hemoglobin distribution was generated by the computation of the fractional occurrence of blood vessels $(h_i = n_i/N_T)$ at each depth interval $\Delta z_i = (z_i - \Delta/2,\ z_i + \Delta/2)$. In our analysis $z_i = i\Delta$ (in millimeters), where $i = 1, 2, 3, \ldots, 20$, $\Delta = 0.05$ mm, n_i is the number of blood vessels counted in the depth interval Δz_i, and N_T is the total number of blood vessels observed in all histologic sections at a skin site. A representative histogram of a type I skin site (Fig. 6) shows good correlation in the dermis ($z > 0.05$ mm) between the hemoglobin distribution h_i deduced from microscopic observation of histologic sections and the corresponding initial temperature distribution $\Delta T(z, t = 0)$.

For the quantitative comparison of histologic observations with computed initial temperature distributions, algebraic terms representing light absorption by melanin $[\Delta T_m(z, t = 0)]$ in the epidermis and hemoglobin within the dermal PWS blood vessels $[\Delta T_b(z, t = 0)]$ are identified by

$$\Delta T(z, t = 0) = \Delta T_m(z, t = 0) + \Delta T_b(z, t = 0). \tag{6}$$

For each biopsied skin site a normalized thermal

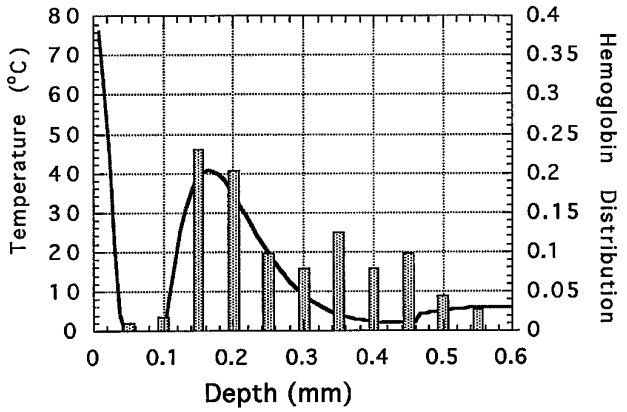

Fig. 6. Hemoglobin distribution (h_i, bars) deduced from microscopic observation of histologic sections and the corresponding initial temperature distribution [$\Delta T(z, t = 0)$, solid line] in a type I skin site.

distribution b_i [Eq. (7)] is computed; b_i represents the degree of blood-vessel heating in each depth interval Δz_i:

$$b_i = \frac{\int_{z_i-\Delta/2}^{z_i+\Delta/2} \Delta T_b(z, t = 0)\mathrm{d}z}{\int_{z_1-\Delta/2}^{z_{20}+\Delta/2} \Delta T_b(z, t = 0)\mathrm{d}z}. \quad (7)$$

The mean depths [Eqs. (8)] computed from hemoglobin (z_h) and thermal (z_b) distributions are compared by the use of Student's paired t-test[29]; for each biopsied skin site z_h and z_b are essentially indistinguishable ($p > 0.94$):

$$z_h = \sum_{i=1}^{i=20} z_i h_i, \qquad z_b = \sum_{i=1}^{i=20} z_i b_i. \quad (8)$$

The square root of the standard variance [σ, Eq. (9)] between h_i and b_i is computed for each biopsied skin site; for type I and type II sites σ was 0.03 and 0.08, respectively, as given by

$$\sigma = \left[\frac{\sum_{i=1}^{20} (h_i - b_i)^2}{20}\right]^{1/2}. \quad (9)$$

Many factors are relevant when comparing hemoglobin h_i and thermal b_i distributions. First, because the light-fluence distribution decreases at deeper skin positions,[30] we expect values of h_i to exceed those of b_i at greater depths (see e.g., Fig. 6). Second, one is not able to exclude a number of potential artifacts in h_i. These artifacts include: (1) vessels that are counted during the computation of h_i may be empty of blood during laser irradiation and thus may not contribute to b_i; (2) the hemoglobin content may not scale uniformly with the number of blood vessels at various depths; and (3) fixing, dehydrating, and embedding the biopsies may introduce tissue shrinkage. In view of these considerations, the correlation found between h_i and b_i in this study is satisfactory. Hence the use of state-of-the-art tissue-processing techniques (e.g., plastic embedding) in combination with novel diagnostic methods[31] may provide a basis for an accurate and objective evaluation of PPTR for the characterization of biological materials.

The authors wish to thank Steven L. Jacques for many helpful discussions. Xiao-jun Wang provided technical assistance with the OLCR measurements of collagen phantoms. Gerald D. Lucassen computed the least-squares fits to the tails of the PPTR signals to determine the value of h. This project was supported by research grants awarded from the Biomedical Research Technology Program (R03-RR06988), the Institute of Arthritis and Musculoskeletal and Skin Diseases (1R29-AR41638-01A1 and 1R01-AR42437-01A1) at the National Institutes of Health, the Whitaker Foundation (9496), and from the Dermatology Foundation to J. S. Nelson and T. E. Milner. Institutional support from the Office of Naval Research, the Department of Energy, the National Institutes of Health, and the Beckman Laser Institute and Medical Clinic Endowment is also gratefully acknowledged. The work of Dennis Goodman was performed under the auspices of the U.S. Department of Energy at the Lawrence Livermore National Laboratory under contract W-7405-Eng-48. Sun Microsystems Computer Corporation provided the resources necessary to compute the inversions. The Office of Academic Computing, University of California, Irvine, provided indispensable technical assistance. Chris Johnston of Amber Engineering generously provided the use of an IR-FPA camera system.

References

1. J. A. Bauer and Th. Sauer, "Cutaneous 10-MHz ultrasound B scan allows the quantitative assessment of burn depth," Burns Therm. Injury **15,** 49–51 (1989).
2. J. M. Schmitt, A. Knuttel, and R. F. Bonner, "Measurement of optical properties of biological tissues by low-coherence reflectometry," Appl. Opt. **32,** 6032–6042 (1993).
3. M. Rajadhyaksha, M. Grossman, D. Esterowitz, R. H. Webb, and R. R. Anderson, "*In vivo* confocal scanning laser microscopy of human skin: melanin provides strong contrast," J. Invest. Dermatol. **104,** 946–952 (1995).
4. H.-A. Crostack, W. Jahnel, E. H. Meyer, and K.-J. Pohl, "Recent developments in non-destructive testing of coated components," Thin Solid Films **181,** 295–304 (1989).
5. D. J. Crowther, L. D. Favro, P. K. Kuo, and R. L. Thomas, "Inverse scattering algorithm applied to infrared thermal wave images," J. Appl. Phys. **74,** 5828–5835 (1993).
6. F. H. Long and T. F. Deutsch, "Pulsed photothermal radiometry of human artery," IEEE J. Quantum Electron. **23,** 1821–1826 (1987).
7. F. H. Long, N. S. Nishioka, and T. F. Deutsch, "Measurement of the optical and thermal properties of biliary calculi using pulsed photothermal radiometry," Lasers Surg. Med. **7,** 461–466 (1987).
8. S. L. Jacques, J. S. Nelson, W. H. Wright, and T. E. Milner, "Pulsed photothermal radiometry of port-wine-stain lesions," Appl. Opt. **32,** 2439–2446 (1993).
9. R. R. Anderson, H. Beck, U. Bruggeman, W. Farinelli, S. L. Jacques, and J. A. Parish, "Pulsed photothermal radiometry in turbid media: internal reflection of backscattered radiation strongly influences optical dosimetry," Appl. Opt. **28,** 2256–2262 (1989).
10. S. A. Prahl, I. A. Vitkin, U. Bruggemann, B. C. Wilson, and R. R. Anderson, "Determination of optical properties of turbid media using pulsed photothermal radiometry," Phys. Med. Biol. **37,** 1203–1217 (1992).
11. I. A. Vitkin, B. C. Wilson, R. R. Anderson, and S. A. Prahl, "Pulsed photothermal radiometry in optically transparent media containing discrete optical absorbers," Phys. Med. Biol. **39,** 1721–1744 (1994).
12. T. E. Milner, D. M. Goodman, B. S. Tanenbaum, and J. S. Nelson, "Depth profiling of laser-heated chromophores in biological tissues by pulsed photothermal radiometry," J. Opt. Soc. Am. A **12,** 1479–1488 (1995).

13. W. J. Cody, "Rational Chebyshev approximations for the error function," Math. Comput. **23,** 631–638 (1969).
14. C. W. Groetsch, *The Theory of Tichonov Regularization for Fredholm Equations of the First Kind* (Pitman, New York, 1984).
15. D. M. Goodman, E. M. Johansson, and T. W. Lawrence, "On applying the conjugate-gradient algorithm to image processing problems," in *Multivariate Analysis: Future Directions,* C. R. Rao, ed. (North-Holland, Amsterdam, 1993).
16. I. E. Frank and J. H. Friedman, "A statistical view of some chemometrics regression tools," Technometrics **35,** 109–148 (1993).
17. M. Stone and R. J. Brooks, "Continuum regression: cross-validated sequentially constructed prediction embracing ordinary least squares, partial least squares, and principal components regression," J. R. Stat. Soc. B **52,** 237–269 (1990).
18. A. Björck, "A bidiagonalization algorithm for solving large and sparse ill-posed systems of linear equations," BIT **28,** 658–670 (1988).
19. P. C. Hansen and D. P. O'Leary, "The use of the *L*-curve in the regularization of discrete ill-posed problems," SIAM J. Sci. Comput. **14,** 1487–1503 (1993).
20. D. Huang, E. A. Swanson, C. P. Lin, J. S. Schuman, W. G. Stinson, W. Chang, M. R. Hee, T. Flotte, K. Gregory, C. Puliafato, and J. G. Fujimoto, "Optical coherence tomography," Science **254,** 1178–1181 (1991).
21. X. Clivaz, F. Marquis-Weible, R. P. Salathé, R. P. Novàk, and H. H. Gilgen, "High-resolution reflectometry in biological tissues," Opt. Lett. **17,** 4–6 (1992).
22. X. J. Wang, T. E. Milner, R. P. Dhond, W. V. Sorin, S. A. Newton, and J. S. Nelson, "Characterization of human scalp hairs by optical low-coherence reflectometry," Opt. Lett. **20,** 524–526 (1995).
23. F. A. Duck, *Physical Properties of Tissue: A Comprehensive Reference Book* (Academic, London, 1990).
24. D. M. Wieliczka, S. Weng, and M. R. Querry, "Wedge shaped cell for highly absorbant liquids: infrared optical constants of water," App. Opt. **28,** 1714–1719 (1989).
25. G. M. Hale and M. R. Querry, "Optical constants of water in the 200-nm to 200-μm wavelength region," App. Opt. **12,** 555–563 (1973).
26. B. B. Doyle and E. R. Blout, "Infrared spectroscopy of collagen and collagen-like peptides," Biopolymers **14,** 937–957 (1975).
27. F. P. Incropera and D. P. DeWitt, *Fundamentals of Heat Transfer* (Wiley, New York, 1985), p. 8.
28. X. J. Wang, T. E. Milner, M. C. Chang, and J. S. Nelson, "Group refractive index measurement of dry and hydrated collagen films using optical low-coherence reflectometry," J. Bio. Opt. **1,** 212–216 (1996).
29. W. H. Press, B. P. Flannery, S. A. Teukolsky, and W. T. Vetterling, *Numerical Recipes in C: The Art of Scientific Computing* (Cambridge U. Press, Cambridge, 1988).
30. D. J. Smithies and P. H. Butler, "Modeling the distribution of laser light in port-wine stains with the Monte Carlo method," Phys. Med. Bio. **40,** 701–731 (1995).
31. X. J. Wang, T. E. Milner, J. S. Nelson, "Characterization of fluid flow velocity by optical Doppler tomography," Opt. Lett. **20,** 1337–1339 (1995).